Institut für Numerische Simulation
Rheinische Friedrich-Wilhelms-Universität Bonn
Wegelerstraße 6 • 53115 Bonn • Germany
phone +49 228 73-3427 • fax +49 228 73-7527
www.ins.uni-bonn.de

Tobias Kluth, Bangti Jin and Guanglian Li

On the Degree of Ill-Posedness of Multi-Dimensional Magnetic Particle Imaging

INS Preprint No. 1718

December 2017

On the Degree of Ill-Posedness of Multi-Dimensional Magnetic Particle Imaging

Tobias Kluth* Bangti Jin† Guanglian Li‡

December 15, 2017

Abstract

Magnetic particle imaging is an imaging modality of relatively recent origin, and it exploits the nonlinear magnetization response for reconstructing the concentration of nanoparticles. Since first invented in 2005, it has received much interest in the literature. In this work, we study one prototypical mathematical model in multi-dimension, i.e., the equilibrium model, which formulates the problem as a linear Fredholm integral equation of the first kind. We analyze the degree of ill-posedness of the associated linear integral operator by means of the singular value decay estimate for Sobolev smooth bivariate functions, and discuss the influence of various experimental parameters. In particular, applied magnetic fields with a field free point and a field free line are distinguished. The study is complemented with extensive numerical experiments.

Keywords: magnetic particle imaging; degree of ill-posedness; equilibrium model; singular value decay; Sobolev smooth bivariate functions.

1 Introduction

Magnetic particle imaging (MPI) is a relatively new imaging modality [10]. The main goal is to reconstruct a spatially dependent concentration of iron oxide nanoparticles by exploiting their superparamagnetic behavior. Measurements are obtained from multiple receive coils where a potential is induced by particles' nonlinear response to the applied dynamic magnetic field using either field free point (FFP) [10] or field free line (FFL) [40] trajectories. These measurements can yield reconstructions with a high spatial/temporal resolution. Since the modality is free from harmful radiation, it is especially beneficial for in-vivo applications.

So far, MPI has been used for preclinical medical applications, and holds a significant potential for clinical applications. One application, already suggested at the beginning of the MPI development, is vascular imaging [10]. In in-vivo experiments, the potential for imaging blood flow was demonstrated using healthy mice [41]. Recently, long-term circulating tracers for monitoring tasks were studied [18]. The high temporal resolution allows tracking medical instruments [13], e.g., in angioplasty [35]. Other applications include cancer detection [43] and cancer treatment by hyperthermia [31].

In practice, MPI is usually modeled by a linear Fredholm integral equation of the first kind. This is motivated by the suppression of particle interactions due to nonmagnetic coating, which allows postulating a linear relationship between particle concentration and the measured potential. However, precisely modeling MPI respectively formulating a physically accurate integral kernel for image reconstruction is still an unsolved problem due to (potentially large) modelling errors in the particle dynamics and data acquisition, e.g., particle relaxation, particle-particle interactions and transfer function for analog filter; we refer the interested reader to the recent survey paper [19] for further details. In the literature, the equilibrium model based on the Langevin function has been used extensively to predict the signal behavior in MPI [22, 24]; see Section 2 below for details on the model, its derivation and the underlying assumptions.

The mathematical study on the MPI model is fairly scarce. The only work on FFP trajectories that we are aware of is the recent work of März and Weinmann [29]. In a 1D setup with FFP trajectories moving

*Center for Industrial Mathematics, University of Bremen, Bibliothekstr. 5, 28357 Bremen, Germany (tkluth@math.uni-bremen.de)

†Department of Computer Science, University College London, Gower Street, London WC1E 6BT, UK (b.jin@ucl.ac.uk, bangti.jin@gmail.com)

‡Institute for Numerical Simulation and Hausdorff Center for Mathematics, University of Bonn, Wegelerstraße 6, D-53115 Bonn, Germany (li@ins.uni-bonn.de)

along a line for the equilibrium model, they [29] showed that in the limit of large particle diameters, the integral kernel is a Dirac-delta function, and thus the imaging problem is actually well-posed. Further, they analyzed in detail a related problem which is independent of the FFP trajectory used, under the assumption that each spatial point is scanned multiple times with nonparallel trajectories. The problem was shown to be severely ill-posed in general, and in the large particle diameter limit, the smoothing property of the forward operator improves with spatial dimension d (and thus the problem is increasingly more ill-posed).

If a FFL is moved by the drive field in its perpendicular direction, the FFL problem can be formulated in terms of Radon transform, followed by a convolution with a kernel involving the mean magnetic moment [23]. However, the theoretical analysis of the inverse problem for general FFL trajectories remains missing.

In this work, we study the degree of ill-posedness of the multi-dimensional equilibrium model via singular value (SV) decay of the associated linear integral operator. Our analysis relies crucially on the SV decay estimate for Sobolev smooth bivariate functions, recently established by Griebel and Li [12], and its extension to less regular bivariate functions. The extension is still unavailable in the existing literature and will be given in this work, and the result is of independent interest. We shall discuss the following three practically important cases separately: nonfiltered model, limit model and filtered model, in order to illuminate the important influences of the experimental parameters, e.g., particle size and kernel regularity of the analog filter. Further, we conduct extensive numerical experiments to complement the analysis. When completing the paper, the authors became aware of the preprint [8], where Erb et al. analyzed a 1D MPI model by decomposing the forward operator, and in particular showed the exponential ill-posedness of the problem. It differs substantially from this work in the main focus (multi-dimensional model) and analytical tools.

The SV decay rate plays an important role in understanding the nature of linear inverse problem (see, e.g., [6, 15, 14]), including MPI. First, it characterizes the degree of ill-posedness of the imaging problem, which determines the resolution limit of the image reconstruction step (given the data accuracy and model accuracy etc.). Second, the analysis also sheds insight into how to improve the resolution by properly changing the experimental setting. Hence, over the past few decades, SV decay estimates have received much interest for a number of inverse problems, especially in the context of computed tomography.

The rest of the paper is organized as follows. In Section 2, we describe the equilibrium model, and in Section 3, the SV decay estimate for Sobolev smooth bivariate functions. Then in Section 4, we analyze the decay rate for the integral operators for nonfiltered and filtered models, and discuss the influence of various factors, e.g., spatial dimensionality d and particle parameter β. In Section 5, we present numerical results to support the analytical results, and finally, in Section 6, we give concluding remarks. Throughout, we denote by C with/without subscript a generic constant which may differ at each occurrence.

2 The equilibrium model

Now we describe the equilibrium model, one prototypical mathematical model for MPI.

2.1 Preliminaries

MPI is inherently a 3D problem, and thus vector valued functions remain 3D even if the domain Ω of the spatial variable x is a subset of a d-dimensional affine subspace $E_d \subset \mathbb{R}^3$. Let $\Omega \subset E_d$, $d = 1, 2, 3$, be a bounded domain with a Lipschitz boundary $\partial\Omega$ in E_d. Further, let $T > 0$ denote the maximal data acquisition time and $I := (0, T)$ the time interval during which the measurement process takes place. The temporal derivative of any function $g : I \to \mathbb{R}^d$ is denoted by $\dot{g}$.

In MPI, the measured signal $v_\ell : I \to \mathbb{R}$, $\ell = 1, \ldots, L$, obtained at $L \in \mathbb{N}$ receive coils, is given by

$$v_\ell(t) = -\int_I \int_\Omega c(x)\tilde{a}_\ell(t-t')\kappa_\ell(x,t)\mathrm{d}x\mathrm{d}t' - \underbrace{\int_I \int_{\mathbb{R}^3} a_\ell(t-t')p_\ell(x)^t \dot{H}(x,t)\mathrm{d}x\mathrm{d}t'}_{=v_{\mathrm{E},\ell}(t)}, \tag{2.1}$$

where the superscript t denotes the transpose of a vector, $c : \Omega \to \mathbb{R}^+ \cup \{0\}$ is the concentration of the magnetic nanoparticles and $\kappa_\ell : \Omega \times I \to \mathbb{R}$, $\ell = 1, \ldots, L$, represent the system functions characterizing the magnetization behavior of nanoparticles, cf. Section 2.2 below. The scalar functions $a_\ell : \bar{I} := [-T :$

$T] \to \mathbb{R}$, $\ell = 1, \ldots, L$, are the kernel functions of the analog filter in the signal acquisition chain, and in practice, they are often band stop filters adapted to excitation frequencies of the drive field (defined below) so as to minimize the adverse influence of the excitation field $v_{\mathrm{E},\ell}$ during digitization. The functions $p_\ell : \mathbb{R}^3 \to \mathbb{R}^3$, $\ell = 1, \ldots, L$, denote the vector field which characterizes the sensitivity profile of the receive coils and can be spatially dependent. Throughout, it is assumed that the applied magnetic field $H : \mathbb{R}^3 \times I \to \mathbb{R}^3$ and the filters $\{a_\ell\}_{\ell=1}^L$ are chosen in a way such that all excitation signals $v_{\mathrm{E},\ell} = 0$, $\ell = 1, \ldots, L$.

Remark 2.1. *The assumption on the excitation signals $\{v_{\mathrm{E},\ell}\}_{\ell=1}^L$ is commonly made when studying the structure of the system functions $\{\kappa_\ell\}_{\ell=1}^L$. However, it may be not fulfilled in MPI applications [37, 20].*

The applied magnetic field $H(x,t)$ can be characterized by a spatially dependent magnetic field $g : \mathbb{R}^3 \to \mathbb{R}^3$ and a time-dependent homogeneous magnetic field $h : I \to \mathbb{R}^3$, and the field $H(x,t)$ is given by their superposition, i.e., $H(x,t) = g(x) + h(t)$. The field g, named *selection field*, ensures that a field-free-region is generated. Generally, g is assumed to be linear such that it can be represented by a matrix $G \in \mathbb{R}^{3\times3}$. The field h, named *drive field*, then moves the field-free-region along a certain trajectory. Two MPI methodologies are distinguished by the field free region, whether a FFP is generated ($\mathrm{rank}(G) = 3$) or a FFL is used ($\mathrm{rank}(G) = 2$). It was also proposed for the FFL approach to rotate the selection field over time such that the FFL is rotated [40], and then the selection field is given by $g : \mathbb{R}^3 \times I \to \mathbb{R}^3$ with $g(x,t) = P(t)^t G P(t) x$ where $P : I \to \mathbb{R}^{3\times3}$ is a rotation matrix for all $t \in I$.

The system functions $\{\kappa_\ell\}_{\ell=1}^L$ can be expressed by the receive coil sensitivities $\{p_\ell\}_{\ell=1}^L$ and the particles' mean magnetic moment vector $\bar{m} : \Omega \times I \to \mathbb{R}^3$ as $\kappa_\ell = \mu_0 p_\ell^t \dot{\bar{m}}$, for some constant μ_0 (magnetic permeability in vacuum). This relation follows from Faraday's law and the law of reciprocity [22]. Then the inverse problem is to find the concentration $c : \Omega \to \mathbb{R}^+ \cup \{0\}$ from $\{v_\ell\}_{\ell=1}^L$:

$$v_\ell(t) = -\int_I \int_\Omega c(x) a_\ell(t - t') \kappa_\ell(x, t') \mathrm{d}x \mathrm{d}t', \quad \text{with } \kappa_\ell = \mu_0 p_\ell^t \dot{\bar{m}}. \tag{2.2}$$

In the model (2.2), the linear dependence on the concentration c is obtained under the assumption that particle-particle interactions can be neglected. However, there is evidence that these interactions can affect the particle signal [28]. The nonlinear dependence is beyond the scope of this work.

2.2 Equilibrium MPI model

To specify the MPI model, it remains to describe the generation of the mean magnetic moment vector $\bar{m}(x,t)$ of nanoparticles. There are several possible models, e.g., Fokker-Plank equation or stochastic Landau-Lifschitz-Gilbert equation [19]. The most extensively studied model in MPI is based on the assumptions that the applied magnetic field $H(x,t)$ is static, the particles are in equilibrium, and $\bar{m}(x,t)$ immediately follows the magnetic field $H(x,t)$. Then by Langevin theory for paramagnetism, $\bar{m}(x,t)$ is given by

$$\bar{m}(x,t) = \mathcal{L}_\beta(|H(x,t)|) \frac{H(x,t)}{|H(x,t)|},$$

where $|\cdot|$ denotes the Euclidean norm of vectors, and $\mathcal{L}_\beta : \mathbb{R} \to \mathbb{R}$ is the Langevin function given by

$$\mathcal{L}_\beta(z) = m_0 \left(\coth(\beta z) - (\beta z)^{-1} \right), \tag{2.3}$$

where β and m_0 are given parameters. The Langevin function $\mathcal{L}_\beta(z)$ captures the nonlinear response to the applied magnetic field. The resulting model is termed as *equilibrium model* below.

Remark 2.2. *Physically, the parameters m_0 and β are determined by the saturation magnetization M_{C} of the core material, the volume V_{C} of the single-domain particle's core, the temperature T_{B}, and Boltzmann constant κ_{B}, i.e., $m_0 = M_{\mathrm{C}} V_{\mathrm{C}}$ and $\beta = \mu_0 m_0 / (\kappa_{\mathrm{B}} T_{\mathrm{B}})$. Note that β also depends on the particle diameter D through m_0. At room temperature 293 K, particles consisting of magnetite with a typical diameter D of 30 nm (20 nm) are characterized by $\beta \approx 2.1 \times 10^{-3}$ (0.6×10^{-3}).*

The Langevin function $L_\beta(z)$ is a smooth approximation to the sign function: for any fixed $0 < \beta < \infty$, it belongs to $C^\infty(\mathbb{R})$, and as $\beta \to \infty$, it recovers the sign function.

Lemma 2.1. *For small z, there holds $\mathcal{L}_1(z) = \frac{1}{3}z - \frac{1}{45}z^3 + \frac{2}{945}z^5 - \frac{1}{4725}z^7 + \ldots$ and for any $z \in \mathbb{R}$, there holds $\lim_{\beta\to\infty} \mathcal{L}_\beta(z) = m_0 \mathrm{sign}(z)$.*

In summary, the inverse problem for the equilibrium model is to recover the spatially dependent concentration c from a system of integral equations:

$$\begin{cases} v_\ell(t) = -\int_I \int_\Omega c(x) a_\ell(t-t') \kappa_\ell(x,t') \mathrm{d}x \mathrm{d}t', \\ \kappa_\ell(x,t) = \mu_0 p_\ell^t \dfrac{\mathrm{d}}{\mathrm{d}t} \left[\dfrac{\mathcal{L}_\beta(|H|)}{|H|} H \right], \end{cases} \tag{2.4}$$

for $\ell = 1, \ldots, L$ and the magnetic field $H : \Omega \times I \to \mathbb{R}^3$ is given by $H(x,t) = g(x) + h(t)$, where $g : \Omega \to \mathbb{R}^3$ and $h : I \to \mathbb{R}^3$. Specifically, for MPI, a common choice is $g(x) = Gx$ and $h(t) = A(\sin(f_i t))_{i=1}^3$, where $A \in \mathbb{R}^{3\times 3}$ is a diagonal matrix with $1 \le \mathrm{rank}(A) \le d$, $f_i > 0$, and a constant matrix $G \in \mathbb{R}^{3\times 3}$ with $\mathrm{tr}(G) = 0$. Below, for the matrix G, we distinguish two cases: (i) G has full rank such that a FFP is generated, and (ii) $\mathrm{rank}(G) = 2$ such that a FFL is generated (only for 3D).

In the model (2.4), all vectors belong to $\mathbb{R}^3$, which reflects the intrinsic 3D nature of the MPI imaging problem. However, for a spatial domain $\Omega \subset \mathbb{R}^d$, $d = 1, 2$, the dimensionality of the vectors and matrices can be taken to be d, by properly restricting to subvectors/submatrices, which is feasible under the assumption $G^{-1}h(t) \in \Omega$, for any $t \in I$ (i.e., field free region is contained in Ω). Specifically, the d-dimensional case, for $d = 1, 2$, can be constructed by assuming that the concentration c is a Dirac δ-distribution with respect to the orthogonal complement of the affine subspace $E_d \subset \mathbb{R}^3$, i.e., $c(x) = c_d(x_1)\delta(x_2)$, where $x = x_1 + x_2$ with $x_1 \in E_d$, $x_2 \in E_d^\perp$, and $c_d : \Omega \subset E_d \to \mathbb{R}^+ \cup \{0\}$. The parametrization of the domain $\Omega \subset E_d$ then allows reformulating the integral in (2.4) in terms of $\Omega_d \subset \mathbb{R}^d$. Given the affine linear parametrization $\Gamma : \Omega_d \to \Omega$, (2.4) can be stated with respect to $\tilde{c}_d : \Omega_d \to \mathbb{R}^+ \cup \{0\}$, $\tilde{c}_d(x) = c_d(\Gamma(x))$. This convention will be adopted in the analysis below, by directly writing $h(t) \in I \to \mathbb{R}^d$ etc.

3 Singular value decay for Sobolev smooth bivariate functions

In this section, we describe SV decay for Sobolev smooth bivariate functions, which is the main technical tool for studying degree of ill-posedness.

3.1 Function spaces

First, we recall Sobolev spaces and Bochner-Sobolev spaces, which are used extensively below. For any index $\alpha \in \mathbb{N}^d$, $|\alpha|$ is the sum of all components. Given a domain $D \subset \mathbb{R}^d$ with a Lipschitz continuous boundary, for any $m \in \mathbb{N}$, $1 \le p \le \infty$, we follow [1] and define the Sobolev space $W^{m,p}(D)$ by

$$W^{m,p}(D) = \big\{ u \in L^p(D) : D^\alpha u \in L^p(D) \text{ for } 0 \le |\alpha| \le m \big\}.$$

It is equipped with the norm

$$\|u\|_{W^{m,p}(D)} = \begin{cases} \Big(\sum\limits_{0\le|\alpha|\le m} \|D^\alpha u\|_{L^p(D)}^p \Big)^{\frac{1}{p}}, \text{ if } 1 \le p < \infty, \\ \max\limits_{0\le|\alpha|\le m} \|D^\alpha u\|_{L^\infty(D)}, \text{ if } p = \infty. \end{cases}$$

The space $W_0^{m,p}(D)$ is the closure of $C_0^\infty(D)$ in $W^{m,p}(D)$. Its dual space is denoted by $W^{-m,p'}(D)$, with $1/p + 1/p' = 1$, i.e., p' is the conjugate exponent of p. Also we use $H^m(D) = W^{m,2}(D)$, and $H_0^m(D) = W_0^{m,2}(D)$. The fractional order Sobolev space $W^{s,p}(D)$, $s \ge 0, s \notin \mathbb{N}$, can be defined by interpolation [1]. It can be equivalently defined by a Sobolev–Slobodeckiĭ seminorm $|\cdot|_{W^{s,p}(D)}$. For $0 < s < 1$, it is defined by

$$|u|_{W^{s,p}(D)}^p := \int_D \int_D \frac{|u(x) - u(y)|^p}{|x-y|^{d+sp}} \mathrm{d}x\mathrm{d}y, \tag{3.1}$$

and the full norm $\|u\|_{W^{s,p}(D)} = (\|u\|_{L^p(D)}^p + |u|_{W^{s,p}(D)}^p)^{1/p}$. For $s > 1$, it can be defined similarly.

We state a result on pointwise multiplication on Sobolev spaces [3, Theorem 7.5].

Theorem 3.1. *Let $D \subset \mathbb{R}^d$, $d = 1, 2, 3$. Assume that s_i, s $(i = 1, 2)$ are real numbers satisfying $s_i \ge s \ge 0$ and $s_1 + s_2 - s > d/2$. Then for some constant $C(s_1, s_2, s, d)$, there holds*

$$\|uv\|_{H^s(D)} \le C(s_1, s_2, s, d) \|u\|_{H^{s_1}(D)} \|v\|_{H^{s_2}(D)} \quad \forall u \in H^{s_1}(D), v \in H^{s_2}(D).$$

Suppose X is a Banach space, with the norm denoted by $\|\cdot\|_X$. Then, for any $p \in \mathbb{N}$, we denote by $H^p(I;X)$ the Bochner space of functions $v : I \to X$ such that $v(t)$ and its weak derivatives (in time) up to order p, i.e., $\dot{v}(t), \ldots, v^{(p)}(t)$, all exist and belong to $L^2(I;X)$. The norm on the space $H^p(I;X)$ is defined by

$$\|v\|^2_{H^p(I;X)} = \sum_{j=0}^{p} \int_I \|v^{(j)}(t)\|^2_X \mathrm{d}t.$$

Then for any $s \geq 0$, we can define $H^s(I;X)$ by means of interpolation, and equivalently using the Sobolev-Slobodeckiĭ seminorm [16]. For example, for $s \in (0,1)$, then the seminorm $|\cdot|_{H^s(I;X)}$ is defined by

$$|v|^2_{H^s(I;X)} = \int_I \int_I \frac{\|v(t_1,\cdot) - v(t_2,\cdot)\|^2_X}{|t_1 - t_2|^{1+2s}} \mathrm{d}t_1 \mathrm{d}t_2,$$

and $\|v\|_{H^s(I;X)} = (\|v\|^2_{L^2(I;X)} + |v|^2_{H^s(I;X)})^{1/2}$. We shall use the case $X = L^2(D)$ extensively. It is well known that the space $H^s(0,T;L^2(D))$ is isomorphic to $H^s(0,T) \times L^2(D)$ and $L^2(D;H^s(0,T))$, i.e., $H^s(0,T;L^2(D)) \simeq H^s(0,T) \times L^2(D) \simeq L^2(D;H^s(0,T))$ (see, e.g., [16, Prop. 1.2.24, p. 25] for the isomorphism $L^2(I;L^2(D)) \simeq L^2(D;L^2(I))$, from which the general case may be derived). Then by [16, Prop. 1.3.3, p. 39], we have $L^2(D;H^{-s}(I)) \simeq H^{-s}(I;L^2(D))$. We shall use these isomorphisms frequently below.

Now we give two results on the composition operator on Bochner-Sobolev spaces, which will be used in Section 4.1. Composition operators on general Bochner-Sobolev spaces seem not so extensively studied (but there are many deep results on Sobolev spaces; see, e.g., [34, Chapter 5]). The first result is about the composition operator on the Bochner space $H^s(I;L^\infty(D))$.

Lemma 3.1. *For $s \geq 0$, let $v \in H^s(I;L^\infty(D)) \cap L^\infty(I;L^\infty(D))$ and $g \in C^k_b(\mathbb{R})$, with $k \geq [s]+1$. Then $g \circ v \in H^s(I;L^\infty(D))$.*

Proof. By the definition of the Sobolev-Slobodeckiĭ seminorm, cf. (3.1), for $0 < s < 1$, since $v \in L^\infty(I;L^\infty(D))$, by the mean value theorem, we have

$$\begin{aligned}
|g \circ v|^2_{H^s(I;L^\infty(D))} &= \int_I \int_I \frac{\|g(v(t_1,\cdot)) - g(v(t_2,\cdot))\|^2_{L^\infty(D)}}{|t_1 - t_2|^{1+2s}} \mathrm{d}t_1 \mathrm{d}t_2 \\
&\leq \int_I \int_I \frac{\sup_{\xi\in\mathbb{R}} |g'(\xi)|^2 \|v(t_1,\cdot) - v(t_2,\cdot)\|^2_{L^\infty(D)}}{|t_1 - t_2|^{1+2s}} \mathrm{d}t_1 \mathrm{d}t_2 \\
&\leq \sup_{\xi\in\mathbb{R}} |g'(\xi)|^2 |v|^2_{H^s(I;L^\infty(D))} < \infty.
\end{aligned}$$

The case $s \geq 1$ follows similarly by the chain rule, e.g., $\frac{\mathrm{d}}{\mathrm{d}t}(g \circ v)(t) = (g' \circ v)\frac{\mathrm{d}}{\mathrm{d}t}v$ etc. □

The second result is about the composition operator for special form Sobolev smooth bivariate functions.

Lemma 3.2. *For any $s, r \geq 0$, let $v(x,t) = f(x) + h(t)$, $f \in H^r(D)$ with $r > d/2$, $h \in H^s(I) \cap L^\infty(I)$ and $g \in C^\infty(\mathbb{R})$. Then $g \circ v \in H^s(I;H^r(D))$.*

Proof. If s is an integer, the chain rule allows verifying the assertion directly. First, for any $0 < s < 1$ and $r \geq 0$, there holds

$$|g \circ v|^2_{H^s(I;H^r(D))} = \int_I \int_I \frac{\|g(v(t_1,\cdot)) - g(v(t_2,\cdot))\|^2_{H^r(D)}}{|t_1 - t_2|^{1+2s}} \mathrm{d}t_1 \mathrm{d}t_2.$$

It remains to bound $\|g(v(t_1,\cdot)) - g(v(t_2,\cdot))\|^2_{H^r(D)}$. By the local Lipschitz continuity of the composition operator [34, Theorem 1, p. 373] and Sobolev embedding, we have

$$\begin{aligned}
\|g(v(t_1,\cdot)) - g(v(t_2,\cdot))\|_{H^r(D)} \leq & C_0 \|v(t_1,\cdot) - v(t_2,\cdot)\|_{L^\infty(D)} \max(\|v(t_1,\cdot)\|_{H^r(D)}, \|v(t_2,\cdot)\|_{H^r(D)}) \\
& + C_0 \|v(t_1,\cdot) - v(t_2,\cdot)\|_{H^r(D)} \leq C_1 \|v(t_1,\cdot) - v(t_2,\cdot)\|_{H^r(D)}.
\end{aligned}$$

This together with the assumption on $v(x,t)$ yields

$$|g \circ v|^2_{H^s(I;H^r(D))} \leq C_1 \int_I \int_I \frac{\|v(t_1,\cdot) - v(t_2,\cdot)\|^2_{H^r(D)}}{|t_1 - t_2|^{1+2s}} \mathrm{d}t_1 \mathrm{d}t_2 < \infty.$$

The case of $s > 1$ can be analyzed similarly using chain rule. □

3.2 Singular value decay

Now we describe our main tool of the analysis, i.e., SV decay estimates for Sobolev smooth bivariate functions. The study of eigenvalues of integral operators with a kernel function has a rather long history. The monographs [33] and [26] contain a wealth of relevant results. However, the results in these works are concerned with two variables defined on the same domain, which cannot handle the integral kernel $\kappa(x,t)$ directly. We shall use the recent result due to Griebel and Li [12], cf. [12, Theorem 3.2], for the nonfiltered model in Section 4.1.

Theorem 3.2. *Suppose that $D \subset \mathbb{R}^d$ satisfies the strong local Lipschitz condition. Let $\kappa(x,y) \in L^2(\Omega, H^s(D))$, $s \geq 0$. Then the SVs σ_n of the associated integral operator satisfy*

$$\sigma_n \leq \operatorname{diam}(D)^s C_{\mathrm{em}}(d,s)^{\frac{1}{2}} C_{\mathrm{ext}}(D,s)^{\frac{1}{2}} \|\kappa\|_{L^2(\Omega,H^s(D))} n^{-\frac{1}{2}-\frac{s}{d}},$$

where the constant $C_{\mathrm{ext}}(D,s)$ depends only on D and s (for Sobolev extension), $C_{\mathrm{em}}(d,s)$ is an embedding constant for $\ell_{\frac{d}{d+2s},1} \hookrightarrow \ell_{\frac{d}{d+2s},\infty}$, and $\operatorname{diam}(D)$ is the diameter of the domain D.

Note that the result in Theorem 3.2 requires $s \geq 0$, which does not cover less regular kernels for the limit model in Section 4.2 below. For general rough kernels, the spectral theory is largely open [33, 26]. We exploit the special structure of the kernel $f(x,t) := |Gx - h(t)|^{-d/2}$ defined on $D \times I$ with $d > 1$ being the dimension of the domain D, and use the proof techniques developed in [33, 12].

To show the decay rate, we make the following assumption.

Assumption 3.1. *Suppose that the matrix $G \in \mathbb{R}^{d\times d}$ is invertible, and the trajectory $h(t) : I \to \mathbb{R}^d$ satisfies the following two properties.*

(i) *There exists C_h such that $C_h := \sup_{t\in[0,T]} |\dot{h}(t)|^{-1} < \infty$.*

(ii) *For any $t \in I$, $G^{-1}h(t) \in D$; and there exists at most N_h distinct $t \in I$ such that $h(t) = Gx$, for any $x \in D$.*

Remark 3.1. *The condition $G^{-1}h(t) \in D$ describes that the FFP moves within the physical domain, and the domain is properly covered by the trajectories. The analysis remains valid if the condition holds for any open subinterval of I. If for all $t \in I$, $G^{-1}h(t) \notin D$, then $|Gx - h(t)|^r$ belongs to $C^\infty(I; L^2(D))$ for smooth trajectories $h(t)$, and the analysis in Section 4.1 applies directly.*

First, by the proof of Lemma 4.1 below, we have $f(x,t) \in L^2(I; L^p(D))$ for any $p \in (1,2)$. Now we define the associated integral operator $\mathcal{S} : L^{p'}(D) \to L^2(I)$ with $f(x,t)$ as its kernel, and its adjoint operator $\mathcal{S}^* : L^2(I) \to L^p(D)$, respectively, by

$$(\mathcal{S}v)(t) = \int_D f(x,t)v(x)\mathrm{d}x \quad \text{and} \quad (\mathcal{S}^*v)(x) = \int_I f(x,t)v(t)\mathrm{d}t.$$

Let $\mathcal{R} : L^{p'}(D) \to L^p(D)$ by $\mathcal{R} = \mathcal{S}^*\mathcal{S}$. By construction, $\mathcal{R}$ is an integral operator with its kernel $R \in L^p(D) \times L^p(D) : D \times D \to \mathbb{R}$ given by

$$R(x,x') = \int_I f(x,t)f(x',t)\mathrm{d}t. \tag{3.2}$$

The next result gives the mapping properties of the operator $\mathcal{S}$. We refer to [1, pp. 221–228] for an introduction to Lorentz spaces $L^{p,\infty}(D)$.

Lemma 3.3. *For $d = 2, 3$, let Assumption 3.1 be fulfilled. Then the following statements hold.*

(i) *For all $q > 2$, the operator $\mathcal{S} : L^q(D) \to L^\infty(I)$ is bounded;*

(ii) *For all $p \in (\frac{2(d-1)}{d}, 2)$ and $q = \frac{2p}{d(2-p)}$, the operator $\mathcal{S} : L^p(D) \to L^q(I)$ is bounded. In addition, $\mathcal{S}$ is compact from $L^2(D)$ to $L^2(I)$.*

Proof. By the proof of Lemma 4.1 below, $v(t) := \|f(\cdot,t)\|_{L^{2-\epsilon}(D)} \in L^\infty(I)$ for any $\epsilon > 0$. Together with [27, Theorem 6.1, p. 99], it implies that $\mathcal{S}$ is bounded from $L^q(D)$ to $L^\infty(I)$ for all $q > 2$.

The proof of assertion (ii) is inspired by the proof of Theorem 8.10 of [27, p. 165]. It relies on Stein-Weiss interpolation theorem (see, e.g., [27, Theorem 8.2, p. 150] and [36, Chapter 5]). First, we claim that there is some constant $C>0$ such that for any $p\in(\frac{2(d-1)}{d},2)$ and $q=\frac{2p}{(2-p)d}$, there holds

$$\|\mathcal{S}\chi_A\|_{L^{q,\infty}(I)}\leq C|A|^{\frac{1}{p}} \tag{3.3}$$

for all measurable subsets $A\subset D$ with finite measure, where χ_A is the characteristic function of A. If the estimate (3.3) holds, then by Stein-Weiss interpolation theorem, $\mathcal{S}$ is bounded from $L^p(D)$ to $L^q(I)$ for all $p\in(\frac{2(d-1)}{d},2)$ and $q=\frac{2p}{d(2-p)}$. Then Theorem 5.4 of [27, p. 83] implies that $\mathcal{S}$ is compact from $L^2(D)$ to $L^2(I)$. Hence, it suffices to prove the claim (3.3).

First, by Hölder's inequality with an exponent $\gamma\in(\frac{1}{q},\frac{1}{p})$, we obtain

$$\begin{aligned}\mathcal{S}\chi_A(t)&=\int_A|Gx-h(t)|^{-\frac{d}{2}}\mathrm{d}x=\int_A|Gx-h(t)|^{-(\frac{d}{2}-\frac{1}{q})}|Gx-h(t)|^{-\frac{1}{q}}\mathrm{d}x\\&\leq\Big(\int_A|Gx-h(t)|^{-(\frac{d}{2}-\frac{1}{q})(1-\gamma)^{-1}}\mathrm{d}x\Big)^{1-\gamma}\Big(\int_A|Gx-h(t)|^{-\frac{1}{q\gamma}}\mathrm{d}x\Big)^{\gamma}.\end{aligned} \tag{3.4}$$

Let $s:=(\frac{d}{2}-\frac{1}{q})(1-\gamma)^{-1}$, and let $B(G^{-1}h(t),\rho):=\{x\in\mathbb{R}^d:|x-G^{-1}h(t)|\leq\rho\}$ be the ball centered at $G^{-1}h(t)$ with a radius ρ satisfying $|B(G^{-1}h(t),\rho)|=|A|$, which implies $|A|=|\mathbb{S}^{d-1}|\rho^d$, where $|\mathbb{S}^{d-1}|$ denotes the area of the unit sphere in $\mathbb{R}^d$. Then by equation (8.33) of [27, p. 154], we have

$$\begin{aligned}&\int_A|x-G^{-1}h(t)|^{-s}\mathrm{d}x-\int_{B(G^{-1}h(t),\rho)}|x-G^{-1}h(t)|^{-s}\mathrm{d}x\\=&\int_{A\backslash B(G^{-1}h(t),\rho)}|x-G^{-1}h(t)|^{-s}\mathrm{d}x-\int_{B(G^{-1}h(t),\rho)\backslash A}|x-G^{-1}h(t)|^{-s}\mathrm{d}x\\\leq&|A\backslash B(G^{-1}h(t),\rho)|\rho^{-s}-|B(G^{-1}h(t),\rho)\backslash A|\rho^{-s}=0.\end{aligned}$$

Consequently,

$$\int_A|x-G^{-1}h(t)|^{-s}\mathrm{d}x\leq\int_{B(G^{-1}h(t),\rho)}|x-G^{-1}h(t)|^{-s}\mathrm{d}x. \tag{3.5}$$

By the choice of γ, $s:=(\frac{d}{2}-\frac{1}{q})(1-\gamma)^{-1}=d\frac{p-1}{p(1-\gamma)}<d$. Thus, in view of the inequality $|Gx-h(t)|\geq\|G^{-1}\|^{-1}|x-G^{-1}h(t)|$, together with (3.5), changing to polar coordinates leads to

$$\begin{aligned}\int_A|Gx-h(t)|^{-s}\mathrm{d}x\leq&\|G^{-1}\|^s\int_{B(G^{-1}h(t),\rho)}|x-G^{-1}h(t)|^{-s}\mathrm{d}x\\\leq&\|G^{-1}\|^s|\mathbb{S}^{d-1}|\int_0^\rho r^{-s}r^{d-1}\mathrm{d}r\\\leq&\|G^{-1}\|^s|\mathbb{S}^{d-1}|\frac{p(1-\gamma)}{d(1-p\gamma)}\rho^{d\frac{1-p\gamma}{p(1-\gamma)}}.\end{aligned}$$

Therefore, with the identity $|A|=|\mathbb{S}^{d-1}|\rho^d$, we arrive at

$$\int_A|Gx-h(t)|^{-s}\mathrm{d}x\leq C(s,\gamma,p)|A|^{\frac{1-p\gamma}{p(1-\gamma)}}.$$

with a constant $C(s,\gamma,p)=\|G^{-1}\|^s|\mathbb{S}^{d-1}|^{\frac{p-1}{p(1-\gamma)}}\frac{p(1-\gamma)}{d(1-p\gamma)}$. This and (3.4) imply

$$\|\mathcal{S}\chi_A\|_{L^{q,\infty}(I)}\leq C(s,\gamma,p)^{1-\gamma}|A|^{\frac{1}{p}-\gamma}\Big\|\Big(\int_A|Gx-h(t)|^{-\frac{1}{q\gamma}}\mathrm{d}x\Big)^{\gamma}\Big\|_{L^{q,\infty}(I)}. \tag{3.6}$$

It remains to estimate the last term in (3.6). Actually, by definition,

$$\begin{aligned}\Big\|\Big(\int_A|Gx-h(t)|^{-\frac{1}{q\gamma}}\mathrm{d}x\Big)^{\gamma}\Big\|_{L^{q,\infty}(I)}&=\Big(\Big\|\int_A|Gx-h(t)|^{-\frac{1}{q\gamma}}\mathrm{d}x\Big\|_{L^{q\gamma,\infty}(I)}\Big)^{\gamma}\\&\leq\Big(\int_A\Big\||Gx-h(t)|^{-\frac{1}{q\gamma}}\Big\|_{L^{q\gamma,\infty}(I)}\mathrm{d}x\Big)^{\gamma}\\&=\Big(\int_A\Big\||Gx-h(t)|^{-1}\Big\|_{L^{1,\infty}(I)}^{\frac{1}{q\gamma}}\mathrm{d}x\Big)^{\gamma}.\end{aligned} \tag{3.7}$$

Next we fix any $x \in A$, and estimate $\big\||Gx - h(t)|^{-1}\big\|_{L^{1,\infty}(I)}$. Let $g(t) := |Gx - h(t)|^{-1}$. Then, under Assumption 3.1, the nonincreasing rearrangement function $g^*(\tau)$ for $\tau \geq 0$ can be bounded by

$$g^*(\tau) \leq 2C_h N_h \tau^{-1}, \tag{3.8}$$

where the rearrangement function $g^*(\tau)$ is defined by

$$\begin{aligned} g^*(\tau) &= \inf\{c : \big|\{t : |g(t)| \geq c\}\big| \leq \tau\} \\ &= \inf\{c : \big|\{t : |h(t) - Gx| \leq c^{-1}\}\big| \leq \tau\}, \end{aligned}$$

by slightly abusing the notation $|\cdot|$ for the Lebesgue measure of a set. Indeed, we have the trivial inclusion $\{t : |h(t) - Gx| \leq c^{-1}\} \subset \cup_{j=1}^{N_x}\{t \in [\max(0, t_{j-1}), \min(t_{j+1}, T)] : |h(t) - h(t_j)| \leq c^{-1}\}$, where the time instances t_j satisfy $h(t_j) = Gx$, for $j = 1, \ldots, N_x \leq N_h$, under the given Assumption 3.1. Further, for any $t \in [t_{j-1}, t_j]$, by the mean value theorem, there exists some $\xi_j \in [t_{j-1}, t_j]$ such that $|h(t) - h(t_j)| = |\dot{h}(\xi_j)(t - t_j)|$, then the assertion (3.8) follows. Consequently

$$\big\||Gx - h(t)|^{-1}\big\|_{L^{1,\infty}(I)} := \sup_{\tau > 0} \tau g^*(\tau) \leq 2C_h N_h.$$

Plugging this into (3.7) yields

$$\Big\|\Big(\int_A |Gx - h(t)|^{-\frac{1}{q\gamma}} \mathrm{d}x\Big)^{\gamma}\Big\|_{L^{q,\infty}(I)} \leq (2C_h N_h)^{\frac{1}{q}} |A|^{\gamma},$$

which, together with (3.6), directly implies

$$\|\mathcal{S}\chi_A\|_{L^{q,\infty}(I)} \leq (2C_h N_h)^{\frac{1}{q}} C(s, \gamma, p)^{1-\gamma} |A|^{\frac{1}{p}}.$$

Upon letting $\gamma = \gamma_0 := \frac{p+q}{2pq}$, we obtain the desired estimate. This completes the proof of the lemma. □

The next lemma shows that the operator $\mathcal{R} : L^q(D) \to L^2(D)$ is compact, for any $q > \frac{2(d-1)}{d}$.

Lemma 3.4. *Under the conditions of Lemma 3.3, for any $q > \frac{2(d-1)}{d}$, $\mathcal{R}$ extends to a compact operator from $L^q(D)$ to $L^2(D)$. Especially, $\mathcal{R}$ is compact on $L^2(D)$.*

Proof. This follows directly from Lemma 3.3 together with a duality argument. □

By Lemma 3.4, the operator $\mathcal{R}$ is nonnegative, compact and self-adjoint on $L^2(D)$. By spectral theory for compact operators [42], it has at most countably many discrete eigenvalues, with zero being the only accumulation point, and each nonzero eigenvalue has only finite multiplicity. Let $\{\lambda_n\}_{n=1}^{\infty}$ be the sequence of eigenvalues (with multiplicity counted) associated to $\mathcal{R}$, which are ordered nonincreasingly, and $\{\phi_n\}_{n=1}^{\infty}$ the corresponding eigenfunctions (orthonormal in $L^2(D)$). Moreover, spectral theory implies

$$\forall v \in L^2(D) : \quad \mathcal{R}v = \sum_{n=1}^{\infty} \lambda_n (v, \phi_n)\phi_n \tag{3.9}$$

with $(\cdot, \cdot)$ being the $L^2(D)$ inner product. Let $q^* = \infty$ for $d = 2$, and $q^* = 4$ for $d = 3$. Then by Lemma 3.3 and [27, Theorem 5.4, p. 83], the eigenfunctions $\{\phi_n\}_{n=1}^{\infty}$ have the following summability: For any $q < q^*$ and any $n \in \mathbb{N}_+$, $\phi_n \in L^q(D)$. This together with the spectral decomposition (3.9) indicates that the spectrum of the operator $\mathcal{R}$ will not change if its domain is restricted to $L^{2+\epsilon}(D)$ for any $0 < \epsilon < 1$.

Now we can extend Theorem 3.2 to the kernel $|Gx - h(t)|^{-d/2}$. This result will be used in Section 4.2. We recall a few concepts, i.e., approximation number and Weyl number, from spectral theory [33]. Given two Banach spaces E and F, the n-th approximation number $a_n(W)$ and the Weyl number $x_n(W)$ of an operator $W \in \mathcal{B}(E, F)$ (i.e., the set of all bounded linear operators from E to F) are defined by

$$a_n(W) := \inf\{\|W - L\|_{\mathcal{B}(E,F)} : L \in \mathfrak{F}(E, F),\ \mathrm{rank}(L) < n\},$$

and

$$x_n(W) := \sup\{a_n(WX) : X \in \mathcal{B}(\ell_2, E), \|X\|_{\mathcal{B}(\ell_2,E)} \leq 1\},$$

respectively, where $\mathfrak{F}(E, F)$ denotes the set of the finite rank operators and WX is just the product of the two operators W and X. Furthermore, the following multiplicative property on Weyl numbers holds, cf. [33, Sections 2.4 and 3.6.2]:

Proposition 3.1. *For all $n \in \mathbb{N}_+$, $X \in \mathcal{B}(E_0, E)$, $W \in \mathcal{B}(E, F)$ and $Y \in \mathcal{B}(F, F_0)$, there holds*

$$x_n(YWX) \leq \|Y\|_{\mathcal{B}(F,F_0)} x_n(W) \|X\|_{\mathcal{B}(E_0,E)}.$$

Theorem 3.3. *Let Assumption 3.1 hold, and $f(x,t) := |Gx - h(t)|^{-d/2}$ with $d = 2, 3$. Then $\lambda_n \leq Cn^{-1/2+\epsilon}$ as $n \to \infty$ for any $\epsilon > 0$.*

Proof. Let $\widetilde{\mathcal{S}} := \mathcal{S}|_{L^{2+\epsilon}(D)}$ for some small fixed $\epsilon > 0$, i.e., the restriction of $\mathcal{S}$ on $L^{2+\epsilon}(D)$. Then by Lemma 3.3(i), the range of $\mathcal{S}$ is $L^\infty(I)$. Hence, we can decompose $\widetilde{S} : L^{2+\epsilon}(D) \to L^{2+\epsilon}(I)$ into $\widetilde{\mathcal{S}} = \mathcal{I}\tilde{\mathcal{S}}$, where $\mathcal{I}$ is the embedding operator from $L^\infty(I)$ to $L^{2+\epsilon}(I)$. The multiplicative property of Weyl numbers x_n in Proposition 3.1 implies

$$x_n(\mathcal{I}\tilde{\mathcal{S}}) \leq x_n(\mathcal{I}) \|\tilde{\mathcal{S}}\|_{\mathcal{B}(L^{2+\epsilon}(D), L^\infty(I))}.$$

By [33, Section 6.3.4, p. 250], there holds $x_n(\mathcal{I}) \leq Cn^{-\frac{1}{2+\epsilon}}$. Thus, we arrive at

$$x_n(\mathcal{I}\tilde{\mathcal{S}}) \leq Cn^{-\frac{1}{2+\epsilon}}.$$

Meanwhile, Lemma 3.3(ii) and a standard duality argument indicate that the dual operator $\mathcal{S}^*$ is bounded from $L^{2+\epsilon}(I)$ to $L^{2+\epsilon}(D)$. Note that $\widetilde{\mathcal{R}} = \mathcal{R}|_{L^{2+\epsilon}(D)}$, and its eigenvalues are $\{\lambda_n\}_{n=1}^\infty$, which can be bounded by the Weyl numbers $x_n(\widetilde{\mathcal{R}})$ according to the eigenvalue theorem for Weyl operators [33, Section 3.6.2]. Hence, we deduce

$$\lambda_n \leq C x_n(\widetilde{\mathcal{R}}) = C x_n(\mathcal{S}^* \mathcal{I} \tilde{\mathcal{S}}) \leq C \|\mathcal{S}^*\|_{\mathcal{B}(L^{2+\epsilon}(I), L^{2+\epsilon}(D))} x_n(\mathcal{I}\tilde{\mathcal{S}}).$$

where the last step is due to Proposition 3.1. Combining the preceding estimates completes the proof. □

Remark 3.2. *The bound in Theorem 3.3 seems not sharp. The sharp one is conjectured to be $O(n^{-1+\epsilon})$. The statement remains valid if the kernel $f(x,t)$ is multiplied by a bounded function. This fact will be used below in Section 4.2.*

4 Degree of ill-posedness

Now we analyze the degree of ill-posedness of the equilibrium MPI model (2.4) via SV decay rate of the associated integral operator, and focus on three cases: (a) nonfiltered equilibrium model, (b) limit model, and (c) filtered equilibrium model. Dependent of the problem setting, the behavior of the forward operator can differ substantially. This was observed in experimental studies [39]. Our analysis below provides insights into these observations. Since the experimental parameters for all the receive coils are comparable in practice, our analysis below focuses on one receive coil, which allows us to simplify the notation. The decay rate given below determines the best possible degree of ill-posedness (i.e., upper bounds on SVs).

4.1 The non-filtered equilibrium model

First, we consider the case in the absence of the temporal analog filter $a(t)$. Then it follows from (2.4) that the integral operator $F : L^2(\Omega) \to L^2(I)$ for the MPI forward problem is given by

$$\begin{cases} v(t) = -\displaystyle\int_\Omega c(x)\kappa(x,t)\mathrm{d}x, \\ \kappa = \mu_0 p^t \dfrac{\mathrm{d}}{\mathrm{d}t}\left[\dfrac{\mathcal{L}_\beta(|H|)}{|H|} H\right], \\ H(x,t) = g(x) + h(t). \end{cases} \tag{4.1}$$

Now we can state our first main result.

Theorem 4.1. *Let $0 < \beta < \infty$, $d = 1, 2, 3$, $h \in (H^s(I))^d$ with $s \geq 1$, $g \in (L^\infty(\Omega))^d$, and $p \in (L^\infty(\Omega))^d$. Then for the operator $F : L^2(\Omega) \to L^2(I)$, the SVs σ_n decay at a rate $\sigma_n \leq Cn^{1/2-s}$.*

Proof. Under the given assumption, the function $H \in H^s(I;(L^\infty(\Omega))^d) \subset L^\infty(I;(L^\infty(\Omega))^d)$, and by Sobolev embedding, $\dot{H}(x,t) = \dot{h}(t) \in (H^{s-1}(I))^d$. Further, by Lemma 2.1, $L_\beta(|z|)/|z| \in C_b^\infty(\mathbb{R})$ is even, and thus by Lemma 3.1, $\frac{L_\beta(|H|)}{|H|} \in H^s(I;L^\infty(\Omega))$ and $\frac{\mathrm{d}}{\mathrm{d}t}\frac{L_\beta(|H|)}{|H|} \in H^{s-1}(I;L^\infty(\Omega))$. Then by Theorem 3.1, $H\frac{\mathrm{d}}{\mathrm{d}t}\frac{L_\beta(|H|)}{|H|}, \frac{L_\beta(|H|)}{|H|}\dot{h} \in H^{s-1}(I;L^\infty(\Omega))$. Now, by product rule, we deduce

$$\begin{aligned}\kappa &= \mu_0 p^t \frac{\mathrm{d}}{\mathrm{d}t}\frac{L_\beta(|H|)}{|H|}H \\ &= \mu_0 p^t \left(H\frac{\mathrm{d}}{\mathrm{d}t}\frac{L_\beta(|H|)}{|H|} + \frac{L_\beta(|H|)}{|H|}\dot{H}\right) \\ &\in H^{s-1}(I;L^\infty(\Omega)) \subset H^{s-1}(I;L^2(\Omega)).\end{aligned} \tag{4.2}$$

The desired assertion follows from Theorem 3.2. □

Remark 4.1. *If $p, g \in (L^\infty(\Omega))^d$, Theorem 4.1 describes the influence of the trajectory $h(t)$ on the decay. For smooth trajectories, i.e., $h(t) \in (C^\infty(I))^d$ (e.g., sinusoidal trajectory, common in experimental setup), the SVs decay exponentially, and thus the inverse problem is severely ill-posed. For nonsmooth trajectories, i.e., triangular trajectory ($h(t) \in (H^{\frac{3}{2}-\epsilon}(I))^d$, for any $\epsilon \in (0,1/2)$), the decay may be slower.*

In Theorem 4.1, we assume $p, g \in (L^\infty(\Omega))^d$ only. It does not account for additional regularity of $\kappa(x,t)$ in x. In practice, it is often taken to be homogeneous/linear, and thus $\kappa(x,t)$ is very smooth in x. This extra regularity can affect the decay rate, which is described next.

Theorem 4.2. *For $d = 1,2,3$, let $0 < \beta < \infty$, $h \in (H^s(I))^d$ with $s > 3/2$, $g \in (H^r(\Omega))^d$, $r > d/2$ and $p \in (C^\infty(\Omega))^d$. Then for the operator $F : L^2(\Omega) \to L^2(I)$, the SVs σ_n decay as $\sigma_n \le Cn^{-(2r-\epsilon)/d}$, for any small $\epsilon \in (0,1/2)$.*

Proof. By Sobolev embedding, for $s > 3/2$, $\dot{H}(x,t) = \dot{h}(t) \in (H^{s-1}(I))^d \subset (L^\infty(I))^d$. Under the given assumptions, $H(x,t) = g(x) + h(t) \in H^r(\Omega;H^s(I)) \subset L^\infty(\Omega;L^\infty(I))$. Since $L_\beta(|z|)/|z| \in C_b^\infty(\mathbb{R})$ (cf. Lemma 2.1), Lemma 3.2 implies $\frac{L_\beta(|H(x,t)|)}{|H(x,t)|} \in H^r(\Omega;H^s(I))$, and $\frac{\mathrm{d}}{\mathrm{d}t}\frac{L_\beta(|H(x,t)|)}{|H(x,t)|} \in H^r(\Omega;H^{s-1}(I)) \subset H^r(\Omega;L^\infty(I))$. Then by Theorem 3.1, $H\frac{\mathrm{d}}{\mathrm{d}t}\frac{L_\beta(|H(x,t)|)}{|H(x,t)|} \in H^{2r-d/2-\epsilon}(\Omega;L^\infty(I))$ and $\frac{L_\beta(|H(x,t)|)}{|H(x,t)|}\dot{h}(t) \in H^r(\Omega;L^\infty(I))$. Then in (4.2), $\kappa \in H^{\min(r,2r-d/2-\epsilon)}(\Omega;L^\infty(I)) \subset H^{2r-d/2-\epsilon}(\Omega;L^2(I))$, where the last step follows from the assumption $r > d/2$. Thus, by Theorem 3.2, the SVs of the adjoint operator decay at $O(n^{-\frac{1}{2}-\frac{2r-d/2-\epsilon}{d}})$. Since the adjoint operator (with respect to the $L^2(I\times\Omega)$ inner product) shares the SVs [11, p. 27, eq. (2.1)], the desired assertion follows. □

By Theorem 4.2, the SVs of F can decay fast for a nonsmooth trajectory $h(t)$, so long as p and g are sufficiently smooth. The regularity requirement might be relaxed by analyzing more precisely pointwise multiplication in mixed spaces, which, however, is beyond the scope of this work. Since $\dot{h}(t)$ and $p(x)$ enter the kernel $\kappa(x,t)$ as pointwise multipliers, if uniformly bounded, they act as bounded operators on $L^2(I)$ and $L^2(\Omega)$, respectively, and the decay rate remains valid [11, p. 27, eq. (2.2)].

4.2 Limit model

It was also reported that the spatial resolution increases with particle diameter D [39, 21] which corresponds to a large β value in the problem formulation. Hence, we analyze the limit case $\beta \to \infty$ below ($m_0 = 1$). First, we derive the expression for the limit integral operator.

Proposition 4.1. *Let $h \in (H^s(I))^d$ with $s \ge 1$, $g \in (L^\infty(\Omega))^d$, and $p \in (L^\infty(\Omega))^d$. For $\beta \to \infty$, there holds*

$$\frac{\mathrm{d}}{\mathrm{d}t}\left(\mu_0 p^t L_\beta(|H|)\frac{H}{|H|}\right) \to \frac{\mathrm{d}}{\mathrm{d}t}\left(\mu_0 p^t \frac{H}{|H|}\right) \quad \text{in } H^{-1}(I;L^2(\Omega)),$$

and the limit integral operator $\widetilde{F}$ of the operator F defined in (4.1) is given by

$$\begin{cases} v(t) = -\displaystyle\int_\Omega c(x)\tilde{\kappa}(x,t)\mathrm{d}x, \\ \tilde{\kappa} = \mu_0 p^t \left(-\dfrac{HH^t}{|H|^3} + \dfrac{1}{|H|}I_3\right)\dot{H}, \\ H(x,t) = g(x) + h(t). \end{cases} \tag{4.3}$$

Proof. First, by the assumptions on g, h and p and Sobolev embedding theorem, $H(x,t) = g(x) - h(t) \in (L^\infty(\Omega \times I))^d$. Then for any $\phi(t) \in H_0^1(I)$ and $\psi(x) \in L^2(\Omega)$, integration by parts yields

$$\begin{aligned}&\int_I \int_\Omega \mu_0 p(x)^t \frac{\mathrm{d}}{\mathrm{d}t}\left[L_\beta(|H(x,t)|)\frac{H(x,t)}{|H(x,t)|}\right]\phi(t)\psi(x)\mathrm{d}x\mathrm{d}t\\ =&-\int_I \int_\Omega \mu_0 p(x)^t L_\beta(|H(x,t)|)\frac{H(x,t)}{|H(x,t)|}\dot{\phi}(t)\psi(x)\mathrm{d}x\mathrm{d}t.\end{aligned}$$

Now it follows from Cauchy-Schwarz inequality that

$$\begin{aligned}&|\int_I \int_\Omega [L_\beta(|H(x,t)|) - \mathrm{sign}(|H(x,t)|)]\mu_0 p(x)^t \frac{H(x,t)}{|H(x,t)|}\dot{\phi}(t)\psi(x)\mathrm{d}x\mathrm{d}t|\\ \le&\mu_0\|p\|_{(L^\infty(\Omega))^d}\int_I \int_\Omega |L_\beta(|H(x,t)|) - \mathrm{sign}(|H(x,t)|)||\dot{\phi}(t)\psi(x)|\mathrm{d}x\mathrm{d}t\\ \le&\mu_0\|p\|_{(L^\infty(\Omega))^d}\|L_\beta(|H(x,t)|) - \mathrm{sign}(|H(x,t)|)\|_{L^2(\Omega\times I)}\|\dot{\phi}\|_{L^2(I)}\|\psi\|_{L^2(\Omega)}.\end{aligned}$$

Since $\|H\|_{L^\infty(\Omega\times I)} < \infty$, by dominated convergence theorem, we deduce

$$\lim_{\beta\to\infty}\|L_\beta(|H(x,t)|) - \mathrm{sign}(|H(x,t)|)\|_{L^2(\Omega\times I)} = 0.$$

By integration by parts again, and density of the product $\psi\phi$ in $H_0^1(I; L^2(\Omega))$, we obtain the assertion. □

Next we analyze the decay rate of the SVs of the limit operator $\widetilde{F}$. First, we give a result on the Sobolev regularity of the function $|Gx - h(t)|^r$, $r > -d/2$.

Lemma 4.1. *Let Assumption 3.1 hold. Then for any $r > -d/2$, the function $f(x,t) = |Gx - h(t)|^r \in H^s(I; L^2(\Omega))$ for any $s < r + d/2$.*

Proof. Let $\epsilon > 0$ be sufficiently small and $r = -d/2 + \epsilon/2$. Since G is invertible, by the relation $|Gx - h(t)| = |G(x - G^{-1}h(t))| \ge \|G^{-1}\|^{-1}|x - G^{-1}h(t)|$ for any fixed $t \in [0,T]$, we have

$$\int_I \int_\Omega |Gx - h(t)|^{-d+\epsilon}\mathrm{d}x\mathrm{d}t \le \|G^{-1}\|^{d-\epsilon}\int_0^T \Big(\int_\Omega |x - G^{-1}h(t)|^{-d+\epsilon}\mathrm{d}x\Big)\mathrm{d}t.$$

Let $B(G^{-1}h(t),\rho) := \{x \in \mathbb{R}^d : |x - G^{-1}h(t)| \le \rho\}$ satisfy that $|B(G^{-1}h(t),\rho)| = |\Omega|$, which implies $|\Omega| = |\mathbb{S}^{d-1}|\rho^d$. By (3.5) with $A := \Omega$, we obtain

$$\int_I \int_\Omega |Gx - h(t)|^{-d+\epsilon}\mathrm{d}x\mathrm{d}t \le \|G^{-1}\|^{d-\epsilon}\int_0^T \Big(\int_{B(G^{-1}h(t),\rho)} |x - G^{-1}h(t)|^{-d+\epsilon}\mathrm{d}x\Big)\mathrm{d}t.$$

Then changing to polar coordinates for the inner integral leads to

$$\begin{aligned}\int_I \int_\Omega |Gx - h(t)|^{-d+\epsilon}\mathrm{d}x\mathrm{d}t &\le \|G^{-1}\|^{d-\epsilon}T\int_0^\rho r^{-d+\epsilon}r^{d-1}\mathrm{d}r|\mathbb{S}^{d-1}|\\ &= \|G^{-1}\|^{d-\epsilon}T\frac{|\Omega|^{\epsilon/d}}{\epsilon}|\mathbb{S}^{d-1}|^{1-\epsilon/d}.\end{aligned} \tag{4.4}$$

This proves $f(x,t) \in L^2(I; L^2(\Omega))$ for all $r > -d/2$. Next, the derivative $\dot{f}$ of $f = |Gx - h(t)|^r$ is given by $\dot{f} = r|Gx - h(t)|^{r-2}\dot{h}(t)\cdot(Gx - h(t))$. Thus, $|\dot{f}| \le r|Gx - h(t)|^{r-1}|\dot{h}(t)|$, which, together with (4.4), implies that for $r = -d/2 + 1 + \epsilon/2$, there holds

$$\|\dot{f}\|_{L^2(I;L^2(\Omega))} \le r\sqrt{\|G^{-1}\|^{d-\epsilon}T\frac{|\Omega|^{\epsilon/d}}{\epsilon}|\mathbb{S}^{d-1}|^{1-\epsilon/d}}\|\dot{h}\|_{L^2(I)}.$$

Thus, $\|f\|_{H^1(I;L^2(\Omega))} < \infty$. By interpolation, for any $-d/2 + \epsilon/2 < r < -d/2 + 1 + \epsilon/2$, there holds $|Gx - h(t)|^r \in H^s(I; L^2(\Omega))$, with $s = r + d/2$. The general case of any $r > -d/2 + 1$ can be analyzed analogously. The desired assertion follows since the constant $\epsilon \in (0, 1/2)$ can be arbitrarily small. □

Lemma 4.1 requires $r > -d/2$, and does not cover the case $r = -d/2$, which is treated next.

Lemma 4.2. *Let Assumption 3.1 hold. Then for any $p \in (1,2)$, the function $f(x,t) = |Gx - h(t)|^{-d/2} \in L^{2-\epsilon}(\Omega; L^p(I))$ for any $\epsilon > 0$.*

Proof. We only need to show

$$g(x) := \int_I |Gx - h(t)|^{-pd/2} \mathrm{d}t \in L^{2/p,\infty}(\Omega) \quad \text{for all } p \in (1,2). \tag{4.5}$$

Note that $L^{2,\infty}(\Omega) \subset L^{2-\epsilon}(\Omega)$ for all $\epsilon > 0$ [9, Section 6.4], and hence, $f(x,t) \in L^{2-\epsilon}(\Omega; L^p(I))$ for any $p \in (1,2)$. Next we prove (4.5). Since $L^{2/p,\infty}(\Omega)$ is a Banach space with a well-defined norm, we deduce

$$\|g\|_{L^{2/p,\infty}(\Omega)} = \Big\| \int_I |Gx - h(t)|^{-pd/2} \mathrm{d}t \Big\|_{L^{2/p,\infty}(\Omega)} \leq \int_I \Big\| |Gx - h(t)|^{-pd/2} \Big\|_{L^{2/p,\infty}(\Omega)} \mathrm{d}t. \tag{4.6}$$

Let $w(x,t) := |Gx - h(t)|^{-pd/2}$. To estimate $\|g\|_{L^{2/p,\infty}(\Omega)}$, we first compute the nonincreasing rearrangement $w^*(\tau,t)$ for any fixed $t \in I$, which, by definition, is defined for all $\tau \geq 0$ by

$$\begin{aligned} w^*(\tau,t) &= \inf\{c > 0 : |\{x \in \Omega : w(x,t) > c\}| \leq \tau\} \\ &= \inf\{c > 0 : |\{x \in \Omega : |Gx - h(t)| < c^{-\frac{2}{pd}}\}| \leq \tau\}. \end{aligned}$$

This and the inclusion relation $\{x \in \Omega : |Gx - h(t)| < c^{-\frac{2}{pd}}\} \subset \{x \in \Omega : |x - G^{-1}h(t)| < \|G^{-1}\| c^{-\frac{2}{pd}}\}$ (due to the trivial inequality $|Gx - h(t)| \geq \|G^{-1}\|^{-1}|x - G^{-1}h(t)|$) yield

$$w^*(\tau,t) \leq \Big(|\mathbb{S}^{d-1}| \|G^{-1}\|^d \tau^{-1} \Big)^{p/2}.$$

Hence, for $t \in I$, we obtain

$$\begin{aligned} \Big\| |Gx - h(t)|^{-pd/2} \Big\|_{L^{2/p,\infty}(\Omega)} &= \|w(x,t)\|_{L^{2/p,\infty}(\Omega)} \leq \sup_{\tau \geq 0} \tau^{p/2} \Big(|\mathbb{S}^{d-1}| \|G^{-1}\|^d \tau^{-1} \Big)^{p/2} \\ &= \Big(|\mathbb{S}^{d-1}| \|G^{-1}\|^d \Big)^{p/2}, \end{aligned}$$

which, in view of (4.6), yields (4.5). This completes the proof of the lemma. □

Now we can state the degree of ill-posedness for the limit problem for FFP trajectories.

Theorem 4.3. *For $\beta \to \infty$, if $p \in (L^\infty(\Omega))^d$, $h \in (H^s(I))^d$ with $s > 3/2$, $d = 2, 3$, for FFP trajectories, the SVs σ_n of the operator $\widetilde{F}$ decay as (for any $\epsilon \in (0, 1/4)$):*

$$\sigma_n \leq \begin{cases} Cn^{-1+\epsilon}, & d = 3, \\ Cn^{-1/4+\epsilon}, & d = 2. \end{cases}$$

Proof. By the Cauchy-Schwarz inequality, there holds $|\tilde{\kappa}| \leq \mu_0 |p| |H|^{-1} |\dot{H}|$. We discuss the cases $d = 2$ and $d = 3$ separately. For $d = 3$, by Lemma 4.1, $|H|^{-1} \in H^{d/2-1-\epsilon}(I; L^2(\Omega))$, and $\dot{H} = \dot{h} \in (H^{s-1}(I))^d \subset (L^\infty(\Omega))^d$, in view of the assumption $s > 3/2$. By Theorem 3.1 and $p \in (L^\infty(\Omega))^3$, we have $|H|^{-1}|\dot{h}| \in H^{d/2-1-\epsilon}(I; L^2(\Omega))$. Then the assertion follows from Theorem 3.2. The case $d = 2$ is similar, since $|\dot{h}| \in L^\infty(I)$ and $|p| \in L^\infty(\Omega)$, we apply Theorem 3.3 to obtain the desired assertion directly. □

Remark 4.2. *Theorem 4.3 shows that for smooth trajectories, the SVs decay as $O(n^{-d/2+1/2+\epsilon})$, i.e., better smoothing property as d increases. This result suggests increasing β to improve the resolution.*

In practice, one can also have FFL trajectories for $d = 3$, where $G \in \mathbb{R}^{3\times 3}$ has only rank 2. Then for any fixed $t \in I$, the kernel function $\tilde{\kappa}(x,t)$ is singular along a line in Ω, instead of only at one single point. We analyze a simplified model to gain insight. Specifically, since $\mathrm{rank}(G) = 2$ and symmetric, by properly changing the coordinate, we may assume that G is diagonal with the last diagonal entry being zero. Then the condition for any fixed $t \in I$, there exists $x \in \Omega$ such that $Gx = h(t)$ implies $h_3(t) = 0$. Then the singular kernel depends only on the first two components essentially. Thus for a cylindrical domain $\Omega = \Omega_{12} \times \Omega_3$ and if $p(x)$ is constant in x_3 variable, the forward operator $\tilde{F}$ can be reformulated as in the 2D FFP trajectories (with a weighted average of the concentration):

$$v(t) = -\mu_0 \int_{\Omega_{12}} \Big(\int_{\Omega_3} c(x) \mathrm{d}x_3 \Big) p(x)^t \left(-\frac{HH^t}{|H|^3} + \frac{1}{|H|} I_3 \right) \dot{H} \mathrm{d}x_1 \mathrm{d}x_2.$$

The next result analyzes the degree of ill-posedness of FFL trajectories under the designate conditions.

Theorem 4.4. *Under the preceding assumptions, for $\beta \to \infty$, for FFL trajectories in 3D, $p \in (L^\infty(\Omega))^3$, and $h(t) \in (H^s(I))^3$ with $s > 3/2$, the SVs σ_n of the operator $\widetilde{F}$ decay as $\sigma_n \le Cn^{-1/4+\epsilon}$, for any $\epsilon \in (0, 1/4)$.*

Proof. In view of the preceding discussions, the proof is completely analogous to Theorem 4.3 for the case $d = 2$. Since $s > 3/2$, by Sobolev embedding, $\dot{H} = \dot{h}(t) \in (H^{s-1}(I))^3 \hookrightarrow (L^\infty(I))^3$. This and Theorem 3.3 yield directly the assertion. □

Remark 4.3. *In Theorems 4.3 and 4.4, the trajectory $h(t)$ belongs to $(H^s(I))^d$, with $s > 3/2$. This restriction comes from the requirement $\dot{h}(t) \in (L^\infty(I))^d$ to simplify the analysis. The estimates in Theorem 4.4 and Theorem 4.3 for $d = 2$ seem conservative, due to suboptimality of the bound in Theorem 3.3.*

4.3 Filtered model

In practice, the signal is first preprocessed by an analog filter to remove the excitation so that the true signal is not lost during digitalization. This can be achieved by a band stop filter. Mathematically, it amounts to convolution with a given kernel $a(t) : \bar{I} := [-T, T] \to \mathbb{R}$ defined by

$$\tilde{\kappa}(x, t) = \int_I \kappa(x, t')a(t - t')\mathrm{d}t' \quad \forall t \in I.$$

However, the precise form of $a(t)$ remains elusive, which constitutes one of the major challenges in mathematical modeling [19]. To analyze the influence of the filtering step on degree of ill-posedness, we recall a smoothing property of the convolution operator [4, Theorem 3]. Below the notation $(\cdot)_+$ denotes the positive part. We refer to [38] for a treatise on Besov spaces $B^s_{p,\theta}(\mathbb{R})$ on the real line $\mathbb{R}$.

Lemma 4.3. *For $-\infty < \ell_1, \ell_2 < \infty$, $1 \le p_1 \le p_2 \le \infty$, $0 < \theta_1, \theta_2 \le \infty$, with $1/p = 1/p_1' + 1/p_2$ and $1/\theta \ge (1/\theta_2 - 1/\theta_1)_+$, then for $f \in B^{\ell_2-\ell_1}_{p,\theta}(\mathbb{R})$ and $g \in B^{\ell_1}_{p_1,\theta_1}(\mathbb{R})$, the convolution $f * g$ exists and*

$$\|f * g\|_{B^{\ell_2}_{p_2,\theta_2}(\mathbb{R})} \le c\|f\|_{B^{\ell_2-\ell_1}_{p,\theta}(\mathbb{R})}\|g\|_{B^{\ell_1}_{p_1,\theta_1}(\mathbb{R})}.$$

Last, we describe the influence of filtering: the SVs σ_n decay faster.

Theorem 4.5. *Suppose that the zero extension of the filter $a(t) : \bar{I} \to \mathbb{R}$ belongs to $B^r_{1,\theta}(\mathbb{R})$, for some $0 < \theta \le \infty$, and the conditions in Theorem 4.1 hold. Then the SVs σ_n of the filtered operator F decay as $\sigma_n \le Cn^{1/2-s-r}$.*

Proof. Let $\bar{\kappa}$ be any bounded extension from $H^{s-1}(I; L^2(\Omega))$ to $H^{s-1}(\mathbb{R}; L^2(\Omega))$, and denote by $\bar{a}$ the zero extension of $a : \bar{I} \to \mathbb{R}$. Then we can extend $\tilde{\kappa}$ from I to $\mathbb{R}$, denoted by $\hat{\kappa}$, by $\hat{\kappa}(x, t) = \int_{\mathbb{R}} \bar{\kappa}(x, t')\bar{a}(t-t')\mathrm{d}t'$. Clearly, the restriction of $\hat{\kappa}(x, t)$ to I coincides with κ, by the construction of the extension $\bar{a}$. This and the fact $H^s(\mathbb{R}) = B^s_{2,2}(\mathbb{R})$ [38, Remark 4, p. 179] imply

$$\begin{aligned}\|\tilde{\kappa}\|_{H^{s+r-1}(I;L^2(\Omega))} &= \|\bar{\kappa} * \bar{a}\|_{H^{s+r-1}(I;L^2(\Omega))} \le \|\bar{\kappa} * \bar{a}\|_{H^{s+r-1}(\mathbb{R};L^2(\Omega))} \\ &\le c\|\bar{\kappa}\|_{H^{s-1}(\mathbb{R};L^2(\Omega))}\|\bar{a}\|_{B^r_{1,\theta}(\mathbb{R})} \le c\|\kappa\|_{H^{s-1}(I;L^2(\Omega))}\|\bar{a}\|_{B^r_{1,\theta}(\mathbb{R})},\end{aligned}$$

where the second inequality is due to Lemma 4.3 and the last due to the bounded extension. Then the assertion follows from Theorem 3.2. □

5 Numerical results

In this section, we illustrate the theoretical results with numerical examples for the non-filtered FFP and FFL cases. We shall not investigate the influence of analog filter, since it is still poorly understood.

5.1 Setting of numerical experiments

In our numerical simulations, we use parameters that are comparable with real experiments. We parameterize problems (4.1) and (4.3) analogously to the Bruker FFP scanner, and obtain the values for the parameters from a public domain dataset [25]. Sinusoidal excitation patterns are used to move the FFP along Lissajous trajectories, which are frequently employed in practice due to its fast coverage of the domain of interest. In the FFP case, it is assumed that the gradient field $g : \mathbb{R}^3 \to \mathbb{R}^3$

is given by a linear function $g(x) = Gx$, with a diagonal matrix $G \in \mathbb{R}^{3\times 3}$, with a vanishing diagonal sum. The drive field $h : I \to \mathbb{R}^3$ is commonly taken to be smooth trigonometric functions, i.e. $h(t) = (A_1 \sin(2\pi f_1 t), A_2 \sin(2\pi f_2 t), A_3 \sin(2\pi f_3 t))^t$, $A_i, f_i > 0$, $i = 1, 2, 3$. By Theorems 4.1 and 4.2, for $0 < \beta < \infty$, the good spatial regularity of the kernel $\kappa(x, t)$ may preclude examining the influence of trajectory smoothness on the SV decay. Nonetheless, we consider also triangular trajectories, i.e., $h(t) = (A_1 \mathrm{tri}(2\pi f_1 t), A_2 \mathrm{tri}(2\pi f_2 t), A_3 \mathrm{tri}(2\pi f_3 t))^t$, $A_i, f_i > 0$, $i = 1, 2, 3$, where the function $\mathrm{tri} : \mathbb{R} \to [-1, 1]$ is defined by

$$\mathrm{tri}(z) = \begin{cases} \frac{2}{\pi}\theta & \theta = (z \bmod 2\pi) \in [0, \pi/2) \\ 2 - \frac{2}{\pi}\theta & \theta = (z \bmod 2\pi) \in [\pi/2, 3\pi/2) \\ -4 + \frac{2}{\pi}\theta & \theta = (z \bmod 2\pi) \in [3\pi/2, \pi/2). \end{cases}$$

We refer to Fig. 1 for an illustration of Lissajous excitation with sinusoidal and triangular trajectories.

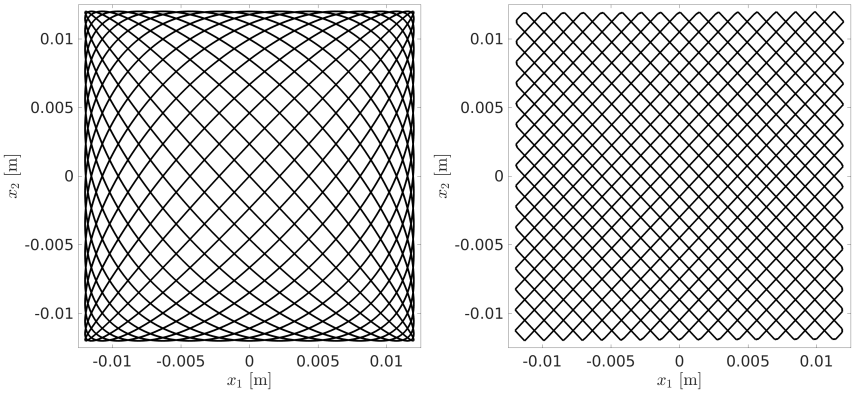

(a) sinusoidal (b) triangular

Figure 1: FFP trajecories Lissajous curve for sinusoidal (a) and triangular (b) excitation in 2D.

The scanner is equipped with three receive coil units, each sensitive to one space-dimension of the mean magnetic moment vector $\bar{m}(x, t)$. The receive coil sensitivities p are assumed to be homogeneous in the simulation, if not otherwise stated. We increase the particle diameter D in order to illustrate the decay behavior as $\beta \to \infty$. The particle's magnetic moment m_0 is set to $m_0 = 1/\mu_0$ in order to avoid diameter-dependent numerical errors, and the remaining particle parameters are chosen following [5].

The forward operators $F, \tilde{F} : L^2(\Omega) \to (L^2(I))^L$ are discretized by a Galerkin method with piecewise constant basis functions on a rectangular partition of the spatial domain Ω and uniform partition of the time interval I. The integrals are computed using a quasi Monte-Carlo integration rule in the spatial variable, with a Halton sequence with 3^d points, for which a good accuracy was reported [30]. It can also approximate singular integrals [32] arising in the limit case. The time integral is computed by a Gaussian quadrature rule, and interval splitting is performed if necessary such that discontinuities lie at the interval boundaries only. MATLAB's built-in function is used to compute SVs of the discrete forward operator.

5.2 Numerical results and discussions

First, we compare the SV decays for the FFP case using sinusoidal excitation patterns moving the FFP along a Lissajous trajectory in the 2D and 3D cases. In all cases, for $d = 1, 2, 3$, the first d receive coils were used to compute the SVs. The parameters used in the numerical simulation are summarized in Table 1. In all the figures, we display only the leading SVs, since the smaller SVs are contaminated by the numerical errors and not reliable. Note that the leading SVs (and singular vectors) play a dominant role in most image reconstruction techniques. The FFP results including the limit cases (2D/3D) are presented in Fig. 2, where for the ease of comparison, the reference decay rates $O(n^{-1/2})$ and $O(n^{-1})$ are also shown. It is observed that as the particle diameter D increases, the decay gets closer to the theoretical predictions from Theorem 4.3. The numerical results for the 2D FFP limit case agree well with the predictions from Theorem 4.3 and the conjecture in Remark 3.2. In the 3D FFP case, the decay is slightly slower than predicted for small ϵ. This might be due to numerical errors, which are larger for

Table 1: Physical parameters used for the simulations. The parameters can be found in: FFP scanner setup [25] and particle parameters [5].

Parameter		**Value**		
Magnetic permeability	μ_0	$4\pi \times 10^{-7}$ H/m		
Boltzmann constant	κ_B	$1.38064852 \times 10^{-23}$ J/K		
Particle				
Temperature	T_B	293 K		
Sat. magnetization	M_C	474000 J/m^3/T		
Particle core diameter	D	$\in \{20, 30, 40\} \times 10^{-9}$ m		
Particle core volume	V_C	$1/6\pi D^3$		
	m_0	$\frac{1}{\mu_0}$		
	β	$\frac{\mu_0 V_\mathrm{C} M_\mathrm{C}}{\kappa_\mathrm{B} T_\mathrm{B}}$		
Geometry	d	1	2	3
FOV	e_1	$[-12.5, 12.5]$ mm	$[-12.5, 12.5]$ mm	$[-12.5, 12.5]$ mm
	e_2	–	$[-12.5, 12.5]$ mm	$[-12.5, 12.5]$ mm
	e_3	–	–	$[-6.5, 6.5]$ mm
Cuboid size	Δx	0.1 mm	0.5×0.5 mm^2	$1.0 \times 1.0 \times 1.0$ mm^3
Scanner FFP case				
Excitation frequencies	f_1	$2.5/102 \times 10^6$ Hz	$2.5/102 \times 10^6$ Hz	$2.5/102 \times 10^6$ Hz
	f_2	–	$2.5/96 \times 10^6$ Hz	$2.5/96 \times 10^6$ Hz
	f_3	–	–	$2.5/99 \times 10^6$ Hz
Excitation amplitudes	A_1	0.012 T/μ_0	0.012 T/μ_0	0.012 T/μ_0
	A_2	–	0.012 T/μ_0	0.012 T/μ_0
	A_3	–	–	0.012 T/μ_0
Gradient strength	$G_{1,1}$	-1 T/m/μ_0	-1 T/m/μ_0	-1 T/m/μ_0
	$G_{2,2}$	-1 T/m/μ_0	-1 T/m/μ_0	-1 T/m/μ_0
	$G_{3,3}$	2 T/m/μ_0	2 T/m/μ_0	2 T/m/μ_0
Measurement time	T	0.04×10^{-3} s	0.653×10^{-3} s	21.54×10^{-3} s
	Δt	0.01×10^{-6} s	0.2×10^{-6} s	0.4×10^{-6} s
Scanner FFL case				
Excitation frequencies	f_1	–	–	–
	f_2	–	$2.5/96 \times 10^6$ Hz	$2.5/96 \times 10^6$ Hz
	f_3	–	–	$2.5/96/25/20 \times 10^6$ Hz
Field rotation	f_rot	–	2604.17 Hz	2604.17 Hz
Excitation amplitudes	A_1	–	–	–
	A_2	–	0.012 T/μ_0	0.012 T/μ_0
	A_3	–	–	0.06 T/μ_0
Gradient strength	$G_{1,1}$	–	0 T/m/μ_0	0 T/m/μ_0
	$G_{2,2}$	–	-1 T/m/μ_0	-1 T/m/μ_0
	$G_{3,3}$	–	1 T/m/μ_0	1 T/m/μ_0
Measurement time	T	–	0.77×10^{-3} s	19.2×10^{-3} s
	Δt	–	0.2×10^{-6} s	0.4×10^{-6} s

3D. Analogous observations can be drawn for triangular excitations in the drive field and when using one single receive coil only. These results can be found in Figs. 3 and 4.

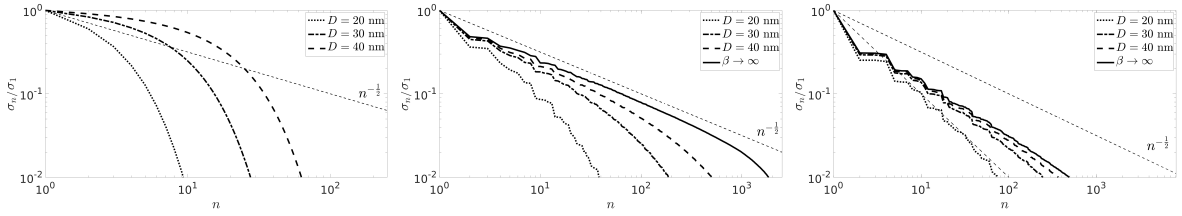

(a) FFP 1D (b) FFP 2D (c) FFP 3D

Figure 2: SV decay for sinusoidal excitation patterns and different particle diameters in (a) 1D, (b) 2D, and (c) 3D domains.

Next we consider the FFL case. In the FFL case, we use a field free line in affine planes of the e_1-e_2-plane, following the approach in [23]. A rotation of the FFL also takes place in this plane using a dynamic selection field $g : \mathbb{R}^3 \times I \to \mathbb{R}^3$ given by $g(x,t) = P(t)^t G P(t) x$ where $P : I \to \mathbb{R}^{3\times 3}$ is

$$P(t) = \begin{pmatrix} \cos(2\pi f_\mathrm{rot} t) & \sin(2\pi f_\mathrm{rot} t) & 0 \\ -\sin(2\pi f_\mathrm{rot} t) & \cos(2\pi f_\mathrm{rot} t) & 0 \\ 0 & 0 & 1 \end{pmatrix}$$

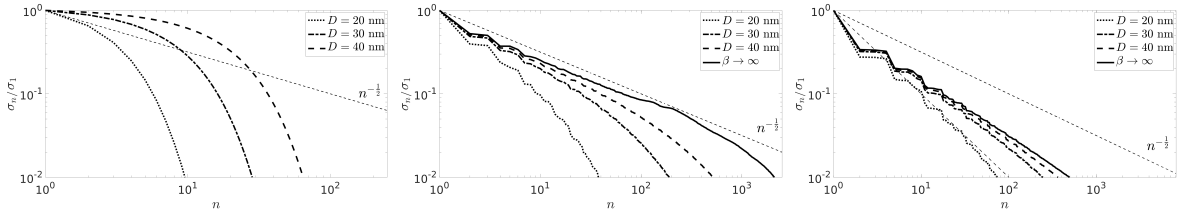

(a) FFP 1D (b) FFP 2D (c) FFP 3D

Figure 3: SV decay for triangular excitation patterns and different particle diameters in (a) 1D, (b) 2D, and (c) 3D domains.

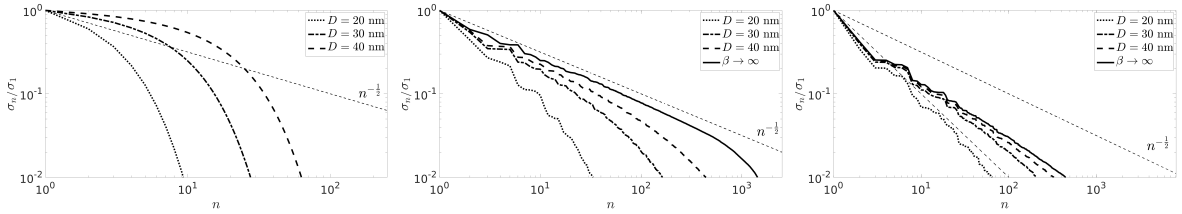

(a) FFP 1D (b) FFP 2D (c) FFP 3D

Figure 4: SV decay for sinusoidal excitation patterns and different particle diameters D, with one single receive coil in (a) 1D, (b) 2D, and (c) 3D domains.

for $f_{\text{rot}} > 0$. A translational movement is performed by using a drive field perpendicular to the FFL at any time $t \in I$. Assuming $G_{1,1} = 0$, the non-rotated FFL is the e_1-axis and we obtain the rotated drive field

$$h(t) = P(t)^t \tilde{h}(t) = A_2 \sin(2\pi f_2 t)(-\sin(2\pi f_{\text{rot}} t), \cos(2\pi f_{\text{rot}} t), 0)^t + A_3 \sin(2\pi f_3 t) e_3.$$

for a non-rotated drive field $\tilde{h}(t) = (0, A_2 \sin(2\pi f_2 t), A_3 \sin(2\pi f_3 t),\ A_2, A_3, f_2, f_3 > 0$. The parameters used to obtain the FFL results are given in Table 1. We use measurement times comparable to the FFP case. The rotation frequency f_{rot} is chosen such that two complete rotations are performed during the whole measurement time in 2D. In 3D a slowly varying field moves the FFL plane in e_3-direction. The corresponding frequency f_3 is chosen such that the field's period is the whole measurement time. In theory, since the rotation matrix $P(t)$ depends smoothly on time t, it does not influence the analysis in Theorem 4.4. The numerical results are summarized in Fig. 5. It is observed that the SVs decay slower, when the particle diameter D increases, just as expected. In 2D we observe a decay rate slightly slower than $O(n^{-1/4})$. The 3D limit case agrees with the prediction in Theorem 4.4 but it does not completely approach the conjectured $O(n^{-1/4})$ or better (the sharp one is conjectured to be $O(n^{-1/2})$, cf. Remark 3.2). In the experiment, one needs to be careful with the parameter choices moving the FFL over space.

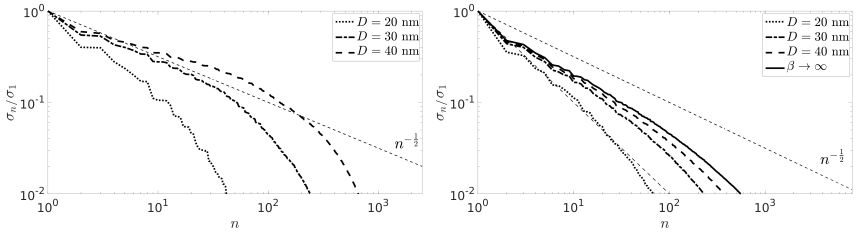

(a) FFL 2D (b) FFL 3D

Figure 5: SV decay for sinusoidal FFL excitation patterns and different particle diameters in (a) 2D and (b) 3D domains.

Last, we compare the FFP and FFL cases. The comparative results in Fig. 6 show clearly the slower SVELTE decays, i.e., less ill-posed, for the FFL case for one example particle diameter in 2D and the limit case in 3D. Equivalently, for a given noise level, there are more significant singular values in the FFL case than in the FFP case, which potentially allows obtaining higher resolution images. These observations confirm the theoretical predictions of Theorems 4.3 and 4.4, and the remarks thereafter.

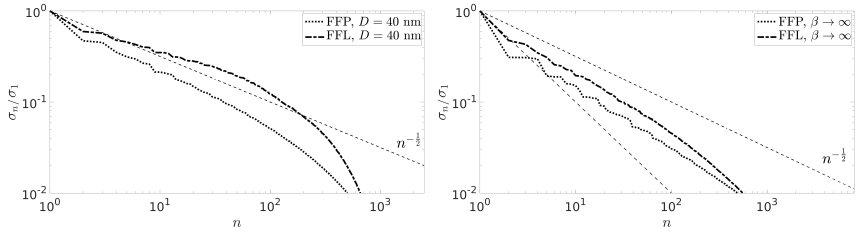

(a) FFP vs. FFL 2D (b) FFP vs. FFL 3D

Figure 6: The comparison of SV decay for the FFP and FFL cases with sinusoidal excitation patterns in (a) 2D and (b) 3D domains.

6 Discussions and concluding remarks

In this work, we have analyzed the non-filtered MPI equilibrium model, and studied the degree of ill-posedness of the forward operator via SV decay for Sobolev smooth bivariate functions. Our analysis gives rise to the following findings. The standard setup in MPI using trigonometric drive field patterns and a linear selection field is a severely ill-posed problem. Even if the temporal dependence is less regular, the spatial regularity (of the linear gradient field) then determines the SV decay. The resolution improvement for larger diameters reported in [39, 21] can be explained by considering the limit case. Two different MPI methodologies, i.e., FFP and FFL, are distinguished in this work. The FFL approach can potentially lead to a less ill-posed problem than the FFP approach, which was also demonstrated in numerical experiments. In the discrete setup, the temporal behavior of the field free line needs to be chosen more carefully to fully exploit the potential benefits predicted by the limit case. In particular, this has to be considered when parameterizing the FFL case with respect to hardware limitations, e.g., rotation frequency [2]. Further, a theoretical result for the filtered problem exhibits a faster SV decay for analog filters with high (temporal) regularity.

The number of theoretical works addressing MPI is still very limited. To the best of our knowledge, the only other theoretical work in the context of inverse problems related to MPI is by März and Weinmann [29]. The authors analyzed a (constructed) non-dynamic problem motivated by the non-filtered time-dependent equilibrium model FFP setup. Similar to our results (Theorem 4.3), the non-dynamic problem shows an increased degree of ill-posedness when increasing the space dimensionality in the limit case. However, the non-dynamic model in [29] is based on certain assumptions on the measurements which are not fulfilled in common MPI experiments with multidimensional FFP trajectories. Taking the equilibrium model for granted, the present work covers the common experimental setups for the FFP and the FFL case. The FFL case has not been considered theoretically before.

The theoretical findings in this work build the basis for several directions of further research of both theoretical and empirical nature. The predicted severe ill-posedness for small particle diameters motivates developing more efficient algorithms based on low-rank approximations of the forward operator. Further, the techniques might also be employed to analyze other more refined models for MPI, which include particle relaxation and particle-particle interactions [19]. Last, for image reconstruction, it is natural to analyze regularized formulations in the context of regularization theory [7, 17].

Acknowledgements

T. Kluth is supported by the Deutsche Forschungsgemeinschaft (DFG) within the framework of GRK 2224/1 “Pi^3 : Parameter Identification - Analysis, Algorithms, Applications”, and G. Li by the Hausdorff Center for Mathematics, University of Bonn.

References

[1] R. A. Adams and J. J. F. Fournier. *Sobolev Spaces*. Elsevier/Academic Press, Amsterdam, second edition, 2003.

[2] A. Bakenecker, T. Friedrich, M. Graeser, J. Stelzner, and T. M. Buzug. Experimental validation of the selection field of a rabbit-sized FFL scanner. *Int. J. Magn. Part. Imag.*, 3(1):article ID 1703013, 5 pp., 2017.

[3] A. Behzadan and M. Holst. Multiplication in Sobolev spaces, revisited. Preprint, arXiv:1512.07379v2, 2017.

[4] V. I. Burenkov. Estimates for Fourier transforms and convolutions in Nikol′skiĭ-Besov spaces. *Trudy Mat. Inst. Steklov.*, 187:31–38, 1989.

[5] R. J. Deissler, Y. Wu, and M. A. Martens. Dependence of Brownian and Néel relaxation times on magnetic field strength. *Med. Phys.*, 41(1):012301–n/a, 2014. 012301.

[6] V. Dicken and P. Maass. Wavelet-Galerkin methods for ill-posed problems. *J. Inv. Ill-Posed Problems*, 4(3):203–221, 1996.

[7] H. W. Engl, M. Hanke, and A. Neubauer. *Regularization of Inverse Problems*. Kluwer, Dordrecht, 1996.

[8] W. Erb, A. Weinmann, M. Ahlborg, C. Brandt, G. Bringout, T. M. Buzug, J. Frikel, C. Kaethner, T. Knopp, T. März, M. M, M. Storath, and A. Weber. Mathematical analysis of the 1D model and reconstruction schemes for magnetic particle imaging. Preprint, arXiv:1711.08074v1, 2017.

[9] G. B. Folland. *Real Analysis: Modern Techniques and their Applications*. John Wiley & Sons, New York, 1999.

[10] B. Gleich and J. Weizenecker. Tomographic imaging using the nonlinear response of magnetic particles. *Nature*, 435(7046):1214–1217, 2005.

[11] I. C. Gohberg and M. G. Kreĭn. *Introduction to the Theory of Linear Nonselfadjoint Operators*. AMS, Providence, R.I., 1969.

[12] M. Griebel and G. Li. On the decay rate of the singular values of bivariate functions. *SIAM J. Numer. Anal.*, page in press, 2017. INS preprint No. 1702, University of Bonn.

[13] J. Haegele, J. Rahmer, B. Gleich, J. Borgert, H. Wojtczyk, N. Panagiotopoulos, T. Buzug, J. Barkhausen, and F. Vogt. Magnetic particle imaging: visualization of instruments for cardiovascular intervention. *Radiology*, 265(3):933–938, 2012.

[14] B. Hofmann and O. Scherzer. Factors influencing the ill-posedness of nonlinear problems. *Inverse Problems*, 10(6):1277–1297, 1994.

[15] B. Hofmann and U. Tautenhahn. On ill-posedness measures and space change in Sobolev scales. *Z. Anal. Anwendungen*, 16(4):979–1000, 1997.

[16] T. Hytönen, J. van Neerven, M. Veraar, and L. Weis. *Analysis in Banach Spaces*. Springer, 2016.

[17] K. Ito and B. Jin. *Inverse Problems: Tikhonov Theory and Algorithms*. World Scientific, Hackensack, NJ, 2015.

[18] A. Khandhar, P. Keselman, S. Kemp, R. Ferguson, P. Goodwill, S. Conolly, and K. Krishnan. Evaluation of PEG-coated iron oxide nanoparticles as blood pool tracers for preclinical magnetic particle imaging. *Nanoscale*, 9(3):1299–1306, 2017.

[19] T. Kluth. Mathematical models for magnetic particle imaging. Preprint, 2017. Available on webpage at `http://www.math.uni-bremen.de/~tkluth/preprint/kluth20171201.pdf`.

[20] T. Kluth and P. Maass. Model uncertainty in magnetic particle imaging: Nonlinear problem formulation and model-based sparse reconstruction. *Int. J. Magnetic Particle Imag.*, 3(2), 2017.

[21] T. Knopp, S. Biederer, T. Sattel, and T. M. Buzug. Singular value analysis for magnetic particle imaging. In *Nuclear Science Symp. Conf. Record, 2008. NSS'08. IEEE*, pages 4525–4529, 2008.

[22] T. Knopp and T. M. Buzug. *Magnetic Particle Imaging: An Introduction to Imaging Principles and Scanner Instrumentation*. Springer, Berlin/Heidelberg, 2012.

[23] T. Knopp, M. Erbe, T. F. Sattel, S. Biederer, and T. M. Buzug. A Fourier slice theorem for magnetic particle imaging using a field-free line. *Inverse Problems*, 27(9):095004, 2011.

[24] T. Knopp, N. Gdaniec, and M. Möddel. Magnetic particle imaging: from proof of principle to preclinical applications. *Phys. Med. Biol.*, 62(14):R124, 2017.

[25] T. Knopp, T. Viereck, G. Bringout, M. Ahlborg, J. Rahmer, and M. Hofmann. MDF: Magnetic particle imaging data format. *Preprint, arXiv:1602.06072*, 2016.

[26] H. König. *Eigenvalue Distribution of Compact Operators*. Birkhäuser Verlag, Basel, 1986.

[27] M. A. Krasnosel'skiĭ, P. P. Zabreĭko, E. I. Pustyl'nik, and P. E. Sobolevskiĭ. *Integral Operators in Spaces of Summable Functions*. Noordhoff International Publishing, Leiden, 1976.

[28] N. Löwa, P. Radon, O. Kosch, and F. Wiekhorst. Concentration dependent MPI tracer performance. *Int. J. Magnetic Particle Imag.*, 2(1), 2016.

[29] T. März and A. Weinmann. Model-based reconstruction for magnetic particle imaging in 2D and 3D. *Inv. Probl. Imag.*, 10(4):1087–1110, 2016.

[30] W. J. Morokoff and R. E. Caflisch. Quasi-Monte Carlo integration. *J. Comput. Phys.*, 122(2):218–230, 1995.

[31] K. Murase, M. Aoki, N. Banura, K. Nishimoto, A. Mimura, T. Kuboyabu, and I. Yabata. Usefulness of magnetic particle imaging for predicting the therapeutic effect of magnetic hyperthermia. *Open J. Med. Imag.*, 5(2):85, 2015.

[32] A. B. Owen. Quasi-Monte Carlo for integrands with point singularities at unknown locations. In *Monte Carlo and quasi-Monte Carlo methods 2004*, pages 403–417. Springer, Berlin, 2006.

[33] A. Pietsch. *Eigenvalues and s-Numbers*. Akademische Verlagsgesellschaft Geest & Portig K.-G., Leipzig, 1987.

[34] T. Runst and W. Sickel. *Sobolev Spaces of Fractional Order, Nemytskij Operators, and Nonlinear Partial Differential Equations*. Walter de Gruyter & Co., Berlin, 1996.

[35] J. Salamon, M. Hofmann, C. Jung, M. G. Kaul, F. Werner, K. Them, R. Reimer, P. Nielsen, A. vom Scheidt, G. Adam, T. Knopp, and H. Ittrich. Magnetic particle/magnetic resonance imaging: in-vitro MPI-guided real time catheter tracking and 4D angioplasty using a road map and blood pool tracer approach. *PLOS one*, 11(6):e0156899–14, 2016.

[36] E. M. Stein and G. Weiss. *Introduction to Fourier analysis on Euclidean spaces*. Princeton University Press, Princeton, N.J., 1971.

[37] K. Them, M. G. Kaul, C. Jung, M. Hofmann, T. Mummert, F. Werner, and T. Knopp. Sensitivity enhancement in magnetic particle imaging by background subtraction. *IEEE Trans. Med. Imag.*, 35(3):893–900, 2016.

[38] H. Triebel. *Interpolation Theory, Function Spaces, Differential Operators*. North-Holland, Amsterdam-New York, 1978.

[39] J. Weizenecker, J. Borgert, and B. Gleich. A simulation study on the resolution and sensitivity of magnetic particle imaging. *Phys. Med. Biol.*, 52(21):6363–6374, 2007.

[40] J. Weizenecker, B. Gleich, and J. Borgert. Magnetic particle imaging using a field free line. *J. Phys. D: Appl. Phys.*, 41(10):105009, 2008.

[41] J. Weizenecker, B. Gleich, J. Rahmer, H. Dahnke, and J. Borgert. Three-dimensional real-time in vivo magnetic particle imaging. *Phys. Med. Biol.*, 54(5):L1, 2009.

[42] K. Yosida. *Functional Analysis*. Springer-Verlag, Berlin-New York, 1980.

[43] E. Y. Yu, M. Bishop, B. Zheng, R. M. Ferguson, A. P. Khandhar, S. J. Kemp, K. M. Krishnan, P. W. Goodwill, and S. M. Conolly. Magnetic particle imaging: a novel in vivo imaging platform for cancer detection. *Nano Letters*, 17(3):1648–1654, 2017.